



Changes in phytoplankton community structure during wind-induced fall bloom on the central Chukchi shelf

Amane Fujiwara¹ · Shigeto Nishino¹ · Kohei Matsuno² · Jonaotaro Onodera¹ · Yusuke Kawaguchi³ · Toru Hirawake² · Koji Suzuki⁴ · Jun Inoue⁵ · Takashi Kikuchi¹

Received: 24 November 2016 / Revised: 8 February 2018 / Accepted: 8 February 2018 / Published online: 20 February 2018
© The Author(s) 2018. This article is an open access publication

Abstract

The recent increasing of atmospheric turbulence has had considerable impact on the oceanic environment and ecosystems of the Arctic. To understand its effect on phytoplankton community structure, a Eulerian fixed-point observation (FPO) was conducted on the Chukchi shelf in fall 2013. Temporal and vertical distributions of the phytoplankton community were inferred from algal pigment signatures. A strong wind event (SWE) occurred during the observation term, and significant convection supplied nutrients from the bottom layer to the surface. Before the SWE, pigment composition in the warmer, less saline, and nutrient-poor surface waters was diverse with low concentration of chlorophyll-*a* (chl*a*). Vertical mixing induced by the SWE weakened the stratification and brought sufficient nutrients to enhance diatom-derived pigment concentrations (e.g., fucoxanthin and chl*c*3), suggesting increases in diatoms. We also developed a model to predict the distribution of major phytoplankton pigment/chl*a* ratios using a profiling multi-wavelength fluorometer (*Multi-Exciter*) with higher spatio-temporal resolution. The *Multi-Exciter* also captured changes in pigment composition with environmental changes at the FPO site and at four observation sites 16 km from the location of the FPO. Furthermore, we investigated the change in grazing rates of the major Arctic copepod *Calanus glacialis* copepodid stage five to assess the interaction between primary and secondary producers during the fall bloom. Increased diatom biomass caused a significant increase in the grazing rate on microphytoplankton (> 20 μm) and a decrease on nanophytoplankton (2–20 μm), indicative of a strong cascade effect because of the reduction of microzooplankton due to the grazing from *C. glacialis*. We conclude that SWEs during fall might affect food webs via the alternation of seasonal succession of phytoplankton community structure.

Keywords Fall bloom · Wind-induced mixing · Phytoplankton community structure · Zooplankton grazing

Introduction

Recent warming of the Arctic Ocean has caused reduction in the area of seasonal sea ice cover; its early break-up in spring and delayed freezing in fall (e.g., Stroeve et al. 2007; Comiso et al. 2008; Markus et al. 2009). Thus, Arctic Ocean ecosystems are facing drastic modification because of these changes. A number of studies have reported shifts in species composition, biomass, and distribution of many trophic level organisms because of the decline of sea ice and related environmental changes (e.g., Grebmeier 2012 and references therein). For example, in phytoplankton communities, a taxonomic shift from large to small has been found in the upper layer of the Canada Basin owing to the nutricline deepening (Li et al. 2009). Earlier sea ice retreat has been found to cause change in the seasonal succession of surface phytoplankton communities in the northern Chukchi

✉ Amane Fujiwara
amane@jamstec.go.jp

¹ Japan Agency for Marine-Earth Science and Technology, 2-15 Natsushima-cho, Yokosuka, Kanagawa 237-0061, Japan

² Faculty of Fisheries Sciences, Hokkaido University, 3-1-1 Minato-cho, Hakodate, Hokkaido 046-8611, Japan

³ Atmosphere and Ocean Research Institute, The University of Tokyo, 5-1-5 Kashiwanoha, Kashiwa, Chiba 277-8564, Japan

⁴ Faculty of Environmental Earth Science, Hokkaido University/JST-CREST, N10 W5, Kita-ku, Sapporo, Hokkaido 060-0810, Japan

⁵ National Institute of Polar Research, 10-3 Midori-cho, Tachikawa, Tokyo 190-8518, Japan

Sea (Fujiwara et al. 2014). Furthermore, enhanced ocean circulation has been reported to stimulate primary productivity in the Eurasian Basin but to reduce it within the Beaufort gyre (Nishino et al. 2011). Changes in secondary producers have also been reported for the Chukchi and adjacent seas. Higher abundance and biomass of mesozooplankton during summers in 2000s than 1990s in the Chukchi Sea is considered to be less ice and warmer temperature (Matsuno et al. 2011). Warmer temperature of less ice condition in the northern Bering Sea is expected to enhance zooplankton grazing activity on phytoplankton (Coyle et al. 2011).

Changes in atmospheric conditions have been reported as well as sea ice conditions. For example, an increase in storm frequency and a northward shift of storm tracks in the Arctic Ocean due to the sea ice loss have been reported (e.g., Serreze et al. 2000; Zhang et al. 2004; Sepp and Jaanus 2011). It is becoming important to take into account the ocean–atmosphere interactions in the Arctic, because recent sea ice loss may lead an increase of wind energy into the surface ocean (Rainville and Woodgate 2009; Martini et al. 2014). In temperate seas, enhanced surface mixing caused by storms could trigger sudden development of phytoplankton blooms because of nutrient enrichment from below the nutricline (Lin 2012; Zhao et al. 2015). Ardyna et al. (2014) documented that the occurrence of fall bloom in the Arctic, rarely seen previously (a single spring bloom is the predominant blooming feature), has increased in pan-Arctic seas because of the growth in the number of stormy days. Because of the short-chained food web in the Arctic, a small change in primary producers can have considerable effect on higher trophic level organisms (Grebmeier et al. 2010). Therefore, it is crucial to comprehend the detailed response of phytoplankton communities to novel blooming characteristics in fall.

To document the physical, chemical, and biological oceanic effects of strong wind, we conducted a fixed-point observation (FPO) on the Chukchi shelf for two weeks (Nishino 2013). Fortunately, a strong wind event (SWE) defined as wind speed exceeds 10 m s^{-1} occurred during the FPO. It persisted for a few days because of the slow movement of an anticyclone over the Siberian Sea (Inoue et al. 2015). Several studies have reported about physical and biogeochemical impacts of the SWE during the FPO. Briefly, the SWE magnitude was sufficiently large to induce internal waves and weaken the vertical stratification (Kawaguchi et al. 2015; Nishino et al. 2015). A significant increase in nutrients from deeper water was found at the surface due to the weakening of the pycnocline. Subsequently, both the chlorophyll-*a* (chl*a*) fraction attributed to large-celled phytoplankton, and the depth-integrated primary production were also found to have increased. Yokoi et al. (2016) examined the taxonomic changes in large phytoplankton ($> 20 \mu\text{m}$) and microzooplankton communities, and reported a remarkable

increase in the number of pennate diatoms after the SWE. Mesozooplankton also responded to the increase in the large-sized phytoplankton ($> 10 \mu\text{m}$) that they feed on (Matsuno et al. 2015). Not only planktonic organisms, but also bacterial abundance and production responded and increased significantly after the SWE (Uchimiya et al. 2016). However, the response of the phytoplankton community structure including small assemblages (e.g., prasinophytes and haptophytes), generally dominate in the surface during strongly stratified season (e.g., Hill et al. 2005; Fujiwara et al. 2014), is still unclear. Since identification of these small assemblages by microscopy requires a high level of taxonomic skills, we used pigment signature as a biomarker to infer the phytoplankton taxonomic composition at the class level (e.g., Jeffrey and Vesik 1997; Wright and Jeffrey 2006). To understand the roles of the fall bloom on biogeochemical cycles and food web, it is important to comprehend the taxonomic response of phytoplankton community structure, because different phytoplankton assemblages play different roles in biogeochemical cycles and ecosystems (e.g., Cushing 1989; Lochte et al. 1993; Sunda et al. 2002; Bopp et al. 2003; Ardyna et al. 2011; Leu et al. 2011). In this study, we also focused on the ecological impact of the fall bloom assessing how increased phytoplankton can transport to the secondary producer, the Arctic copepod *Calanus glacialis*, the key species in the Chukchi Sea, by measuring their grazing rate on phytoplankton. Integrating the knowledge of predator–prey interactions is essential to comprehend recent Arctic changes in ecosystem. Hence we aimed to evaluate the response of phytoplankton community structure and zooplankton grazing activity on the increased phytoplankton to short-term environmental changes during the fall bloom.

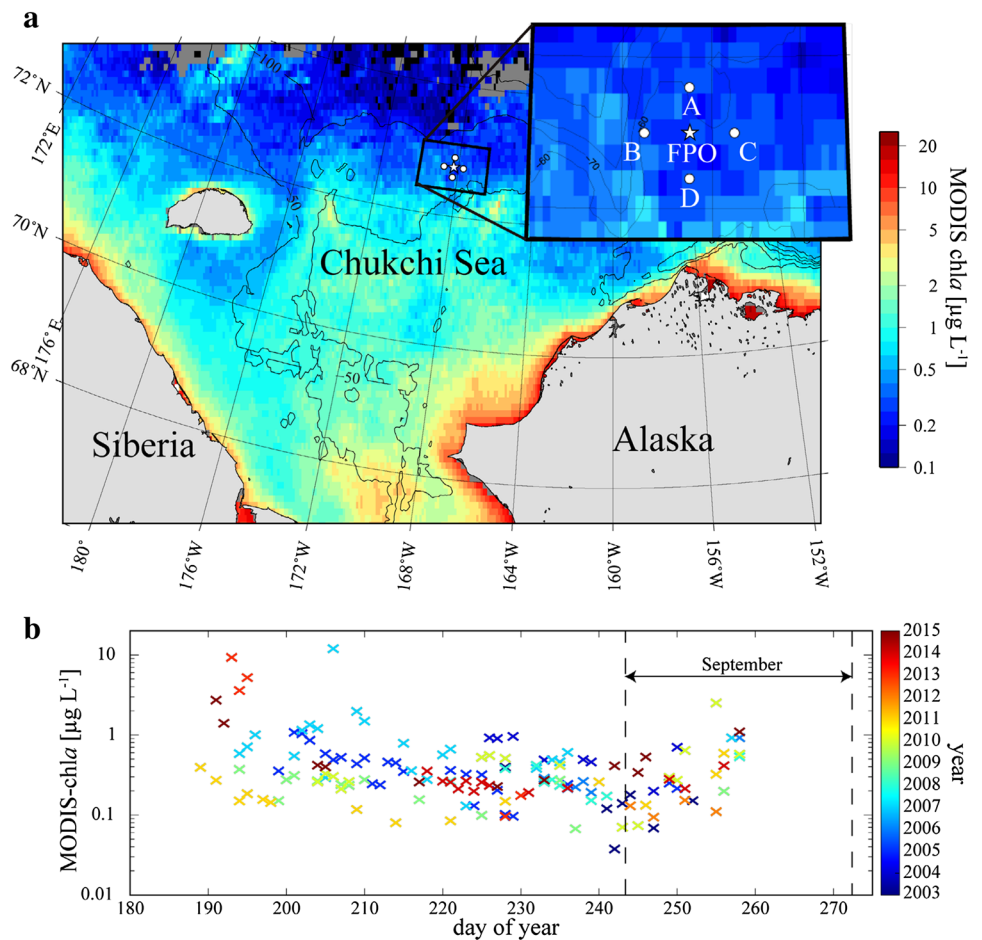
Materials and methods

Cruise summary and water sampling

The FPO site was located at 72.75°N , 168.25°W (Fig. 1a). We remained on station at the FPO site from September 10–25, 2013 and revisited on September 30, during the cruise of *R/V Mirai* (JAMSTEC). CTD observations and routine water sampling were conducted every 6 h at the FPO site (00:00, 06:00, 12:00, and 18:00 UTC). In addition, four observation sites (sub-FPO sites; stations A, B, C, and D) were set 16 km from the FPO site and CTD profiles were conducted between the FPO site samplings. On most CTD casts, a multi-spectral excitation/emission fluorometer (*Multi-Exciter*, JFE-Advantech Co. Ltd.) was attached to the CTD frame to measure the vertical profile of chl*a* fluorescence.

Water samples were collected using a clean plastic bucket for surface samples and 12-L Niskin-X bottles for each

Fig. 1 **a** Location of the sampling domain colored with climatologic mean *chl_a* derived by Aqua-MODIS (2003–2015). The central station (star) is the main FPO site where observations were conducted every 6 h. Sub-FPO stations 16 km from the FPO site are denoted A, B, C, and D (circles). **b** Time series of satellite-derived *chl_a* at the FPO site from 2003 to 2015. Color scale indicates year of the data plots



standard collection depth (5, 10, 20, 30, 40, 45, and 50 m) and optical depth (38, 14, 7, 4, 1, 0.6% relative to surface photosynthetically available radiation, PAR), which were attached to the CTD/Carousel sampler. The temperature and salinity (defined by the dimensionless practical salinity scale) were measured using a thermometer and a Guildline AUTOSAL salinometer, respectively, or by a CTD system (SeaBird Electronics Inc., SBE 9plus). Nutrient concentrations (nitrate, nitrite, ammonia, phosphate, and silicate) were determined onboard using auto-analyzers (QuAatro, SEAL Analytical) within 24 h after sampling according to the GO-SHIP Repeat Hydrography Manual (Hydes et al. 2010) using the Reference Materials of Nutrients in Seawater (Aoyama and Hydes 2010; Sato et al. 2010). Total alkalinity of the water was measured using a spectrophotometric system (NIPPON ANS, Inc.) and the scheme of Yao and Byrne (1998). We calculated the fraction of freshwater contents (i.e., the sea ice meltwater, f_{SIM} , and other freshwater, f_{OF} , carried by the water of Pacific origin) from the values of total alkalinity and salinity following the method of Yamamoto-Kawai et al. (2005), and the endmembers of salinity and total alkalinity were obtained from Nishino et al. (2016). We conducted the measurement of vertical profile

of PAR using a PRR-800 spectroradiometer with a freefall profiler (Biospherical Inc.).

Total *chl_a* concentration was measured at each target depth by filtering 300 mL of seawater onto Whatman GF/F glass fiber filter (25 mm diameter) immediately after the sampling. The filters were soaked in DMF for 24–48 h (Suzuki and Ishimaru 1990), and the *chl_a* concentrations were measured using a fluorometer (10-AU, Turner Design).

Samples for analysis of phytoplankton pigments (chlorophylls and carotenoids) were collected from six or seven depths every FPO observation day at 18:00 UTC (09:00 local time). Sample water (2.2 L) was filtered onto a GF/F filter (25 mm diameter) and stored in liquid nitrogen for 3 months until analysis in the laboratory. The filter samples were soaked and sonicated in 3 mL of N, N-dimethylformamide (DMF) (Suzuki et al. 2002). Then, the extracted algal pigments were separated by HPLC following the method of van Heukelem and Thomas (2001). The pigments used for the analysis were chlorophyll-*c*3 (*chl_c3*), chlorophyll-*c*1 + *c*2 + magnesium divinyl pheoporphyryn a5 monomethyl ester (*chl_c1 + c2 + MgDVP*), peridinin (*peri*), 19'-hexanoyloxyfucoxanthin (*hex*), fucoxanthin (*fuco*), 19'-butanoyloxyfucoxanthin (*but*), diadinoxanthin

(diadino), alloxanthin (allo), zeaxanthin (zea), prasinoloxanthin (prasi), lutein (lut), chlorophyll-*b* (chl*b*), and chl*a*. In this study, we simply interpreted pigment/chl*a* ratios as proxy of taxonomic composition in combination with cluster analysis (see “statistical analysis” section for details), and inferred the temporal and vertical distribution of taxonomic composition (Hill et al. 2005; Fujiwara et al. 2014).

Measurement of high-resolution pigment distribution using *Multi-Exciter*

High-performance liquid chromatography (HPLC) pigment signature is used widely to infer phytoplankton taxonomic composition at the class level (reviewed in Jeffrey and Vesk 1997; Wright and Jeffrey 2006). Several studies have used HPLC pigment signatures to assess the algal taxonomic composition in Arctic seas (e.g., Hill et al. 2005; Coupel et al. 2012, 2015; Fujiwara et al. 2014; Alou-Font et al. 2013; Vidussi et al. 2004), including the Chukchi Sea. However, in the absence of direct measurements of phytoplankton pigment, taxonomic composition has also been derived based on excitation/emission fluorescence spectra (Yentsch and Yentsch 1979; Yentsch and Phinney 1985). Both laboratory and in situ observations have successfully revealed its practical use in identifying or inferring algal community structures (e.g., MacIntyre et al. 2010; Houliez et al. 2012; Kuwahara and Leong 2015; Wang et al. 2016). An in situ multi-excitation fluorometer is a powerful tool for inferring vertical distribution of phytoplankton community structure with high resolution. However, the spectral fluorescence method still has some limitations when applied to in situ observations. For example, the instrument must be calibrated using isolated algal cultures from the study area either before or after observation (Wang et al. 2016). Fortunately, as mentioned above, several studies have referred to the relationship between phytoplankton pigment and taxonomic composition in the Chukchi Sea. Thus, the derivation of pigment signatures is considered sufficient to infer the distribution of phytoplankton communities in the western Arctic Ocean.

The *Multi-Exciter* (JFE-Advantech Inc.), which measures fluorescence response (emission) between 630 and 1000 nm excited at nine wavelengths (375, 400, 420, 435, 470, 505, 525, 570, and 590 nm), is designed to derive temporally or vertically continuous distribution of phytoplankton taxa. Instead of calibration with pure culture samples (*Chaetoceros* sp., *Nannochloropsis* sp., and *Microcystis* sp. are used as default reference groups), we developed a model to derive accessory pigment/chl*a* ratios by quantifying the relationship between fluorescence spectra and HPLC pigments/chl*a* ratios obtained at the same depth. The development of the model was based on an empirical orthogonal function (EOF) analysis of the fluorescence spectra. Several previous studies have successfully modeled water constituents, chl*a*

or phytoplankton community/size composition using EOF analysis of spectral optical signatures, such as remote-sensing reflectance and absorption (Craig et al. 2012; Bracher et al. 2015; Wang et al. 2015). Similarly, we extracted the dominant modes of excitation spectra from the EOF analysis using the MATLAB statistical toolbox (MathWorks Inc.). To minimize the effect of chl*a* concentration, which directly affects the fluorescence spectral shape and magnitude, the spectra were standardized by subtracting the mean and dividing by the standard deviation. Then, the variability of the spectral shapes became comparable with the pigment/chl*a* ratios. Chl*c*3, peri, but, fuco, hex, pras, allo, and chl*b* were chosen for the modeling of their ratios against chl*a*. The partial regression coefficients were selected by stepwise method such that all coefficients were statistically significant (*t* test, *p* < 0.05).

Chl*a* from satellite ocean color data

Aqua-MODIS level-3 standard mapped images of the spectral remote-sensing reflectance (R_{rs}) data (daily and 9 km resolution) were acquired from Goddard Space Flight Center/Distributed Active Archive Center, NASA. Using the continuous time series R_{rs} data (2003–2015), we derived chl*a* concentration from the Arctic OC4L algorithm (Cota et al. 2004), which was optimized for the optical properties of phytoplankton in the Arctic Ocean. September climatologic mean chl*a* were also computed for the Chukchi Sea (Fig. 1a).

Statistical analysis

To group samples of similar pigment composition, cluster analysis was conducted for accessory pigment/chl*a* ratios. This method has been used widely for dividing large volumes of pigment data into several groups (e.g., Hill et al. 2005; Fujiwara et al. 2014; Goés et al. 2014; Isada et al. 2015). For clustering, the unweighted pair group method using arithmetic averages (UPGMA) algorithm with Euclidean distance was chosen following Isada et al. (2015). Cluster analysis was also performed for the pigment/chl*a* ratios predicted by the *Multi-Exciter*, but the k-means clustering method was applied to divide the sample into the same number of cluster as the in situ clusters. The optimum number of cluster was determined using Calinski–Harabasz index (Calinski and Harabasz 1974).

To illustrate the similarity of environmental variables coincident with pigment samples, we conducted a principal component analysis (PCA). Temperature, salinity, total inorganic nitrogen (TIN = nitrate + nitrite + ammonia), phosphate, silicate, f_{OF} , f_{SIM} , and PAR were used as the inputs of the PCA after standardization. Temporal and vertical changes of environmental properties were assessed using

the PCA scores. These statistical analyses were performed using the MATLAB statistical toolbox.

Grazing rate of *Calanus glacialis* C5

Incubation experiments to assess temporal changes in the grazing activity of *C. glacialis* copepodid stage five (C5), which is a key zooplankton species and one of the most abundant species within the region, were conducted twice before the SWE (September 12 and 16) and twice after the SWE (September 24 and 25) using an on-deck incubator. Prior to the water sampling for the incubation, we determined the maximum chl a fluorescence depths using a CTD equipped with a fluorometer. Then, seawater was collected from the layer of maximum chl a fluorescence and dispensed into an acid-rinsed 20-L polyethylene bottle. The sample water was divided into 2.3-L acid-cleaned and Milli-Q rinsed polycarbonate bottles, screened with 330 μm mesh to remove mesozooplankton. *Calanus glacialis* C5 individuals were collected using ring net (mouth diameter 80 cm, mesh size 335 μm) with a 2-L cod-end. Collected zooplankton was retained in ~ 1000 mL of cool filtered seawater prior to being placed into an incubation bottle. Active, freshly collected individuals of *C. glacialis* C5 were chosen and placed in an incubation bottle, one individual per bottle. Each incubation bottle was then sealed with Parafilm, after confirming no bubbles were inside the bottle, and tightly capped. We set two treatments and two control bottles (without copepods) and incubated them for 24 h. During the experiment, the temperatures of the bottles were controlled by running surface water over them, and the light condition was adjusted to 7% relative to surface PAR to be close to the optical depth of chl a maximum. Chl a concentration was measured before and after the incubation for total, > 20 , 2–20, and < 2 μm particles by filtering 500 mL of water through a 20, 2 μm polycarbonate filters and 0.7 μm GF/F filter (47 mm diameter, Whatman), and concentrations were measured using the fluorometer as described in “Cruise summary and water sampling” section. Then, the grazing rates for each size of chl a were calculated following the method of Dagg et al. (2006).

Results

Times series of environmental variables

At the beginning of the FPO, the water column was strongly stratified by both temperature and salinity, and it showed a clear two-layered structure (surface mixed layer was ~ 25 m) (Fig. 2b, c). The upper layer temperature was > 2.5 $^{\circ}\text{C}$ and the salinity was < 31.5 . The water mass classification during the FPO is shown in Fig. 2j modified from Itoh et al.

(2015) for the FPO considering the large fresh water fraction attributed to sea ice meltwater (f_{SIM}). The surface water is categorized as sea ice meltwater (SIMW) (Fig. 2j). The low salinity was coincident with relatively large amounts of f_{SIM} (> 0.02) (Fig. 2g). In contrast, the lower layer temperature was near freezing (< -1 $^{\circ}\text{C}$) and its salinity was ~ 32.8 . The water mass around pycnocline was Bering shelf water (BSW), and bottom water was Pacific winter water (PWW) (Fig. 2j). Both the thermocline and the halocline were located between depths of 20–30 m, where PAR relative to the surface was 3–10%. Vertical profiles of TIN (Fig. 2d) and phosphate (Fig. 2e) followed those of temperature and salinity with depletion in the upper layer and 2–3 magnitudes higher in the lower layer. Silicate generally exhibited a profile similar to the other two nutrients but a subsurface maximum occasionally appeared around the pycnocline with relatively higher f_{OF} (> 0.03) (Fig. 2f, h).

During the FPO term, we observed two occasions when the wind exceeded 10 m s^{-1} : September 14 (257, Julian day) and September 19–21 (262–264, Julian day) (Fig. 2a). Since the major biological responses were found after the stronger and longer second wind event, we hereafter call the second event as SWE in this paper. The strong wind was also recorded at the other four sites around the FPO. We found the apparent responses of the marine environmental variables to the strong wind. The pycnocline weakened after the first strong wind (Fig. 2b, c) as a result of the enhanced internal gravity waves (Nishino et al. 2015; Kawaguchi et al. 2015). Furthermore, the temperature and salinity in the upper layer showed a slight decrease and increase, respectively. The temperature decrease and salinity increase were accelerated by the strong mixing in the upper layer on September 19. As the salinity increased, f_{SIM} in the upper layer decreased (Fig. 2g), and SIMW changed to BSW (Fig. 2j). It was remarkable that nutrients in the upper layer showed different responses; TIN did not change significantly (Fig. 2d, j) but phosphate (Fig. 2e) revealed a significant increase and silicate showed a significant decrease (Fig. 2f). The response of chl a was similar to that of phosphate, which showed a gradual increase from ~ 0.3 to ~ 1.0 mg m^{-3} in the upper layer after the SWE (details are described in “Short-term changes in phytoplankton groups” section). Both pre-bloom chl a (< 0.5 $\mu\text{g L}^{-1}$) and fall bloom chl a (~ 1.0 $\mu\text{g L}^{-1}$) were similar magnitude of satellite-derived chl a (Fig. 1a, b).

Short-term changes in phytoplankton groups

Inference of taxonomic compositions

Cluster analysis was applied to the pigment/chl a ratios, and we divided the phytoplankton community into three groups with dissimilarity criteria = 0.114 (Fig. 3a). The clustered groups showed clear distribution differences with date and

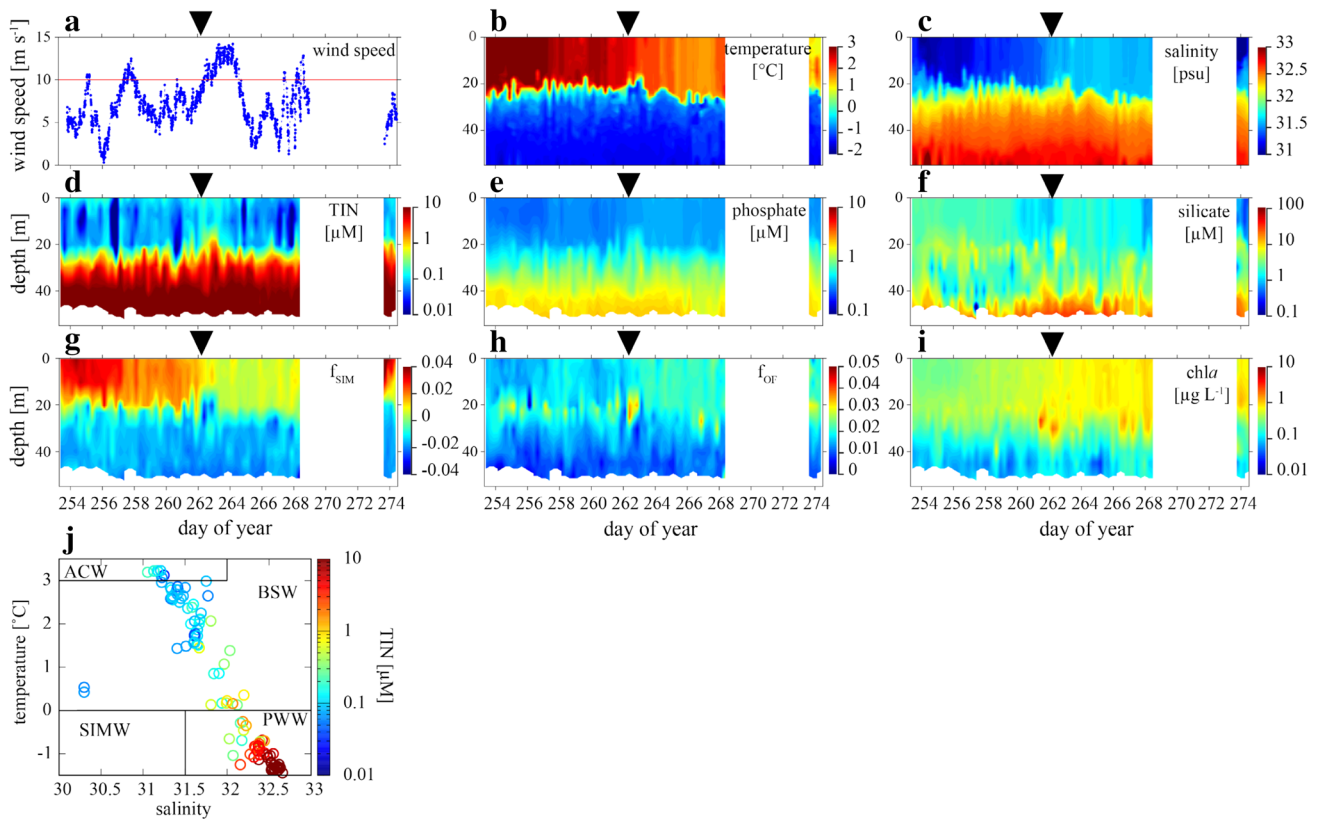


Fig. 2 Time series of **a** wind speed, **b** temperature, **c** salinity, **d** TIN, **e** phosphate, **f** silicate, **g** f_{SIM} , **h** f_{OF} , and **i** chl *a* during the FPO term. Red solid line in **(a)** indicates 10 m s^{-1} . Black triangles denote onset of the SWE. Temperature/salinity diagram is also provided in panel

(j). TIN is indicated by the color scale. Black lines denote the boundary of the different water masses. The water masses are: *ACW* Alaskan coastal water, *BSW* Bering shelf water, *SIMW* Sea ice melt water, *PWW* Pacific winter water

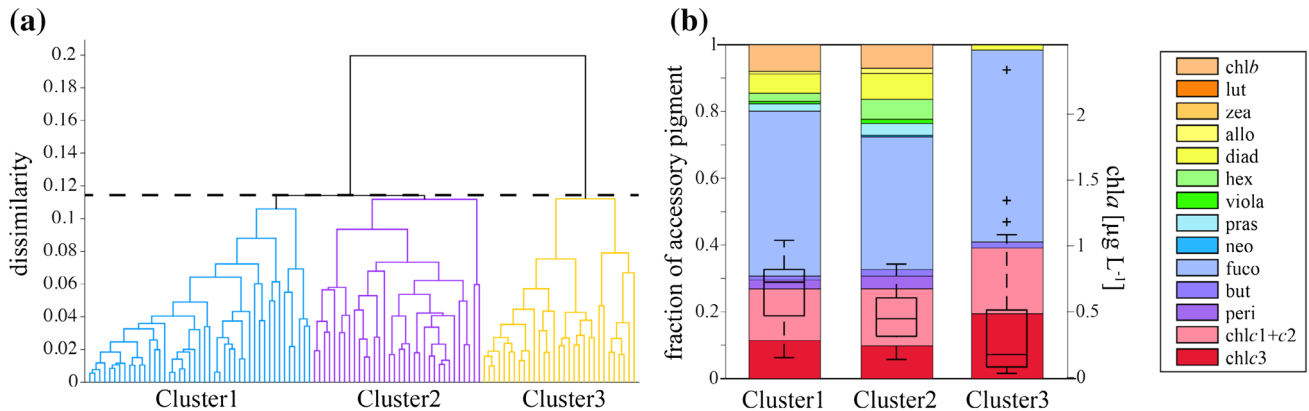


Fig. 3 **a** Dendrogram of cluster analysis based on the UPGMA and Euclidian distance. Colors represent cluster groups divided with dissimilarity criteria = 0.114 (dashed line) and **b** median fractional contribution of accessory pigments to total pigment concentration for

each cluster. Boxplots of chl *a* concentration for the clusters are also provided (right axis) indicating values of median (horizontal bars), 25 and 75% quartiles (box ranges), confidence intervals (whiskers), and outliers (crosses)

depth (Fig. 4). Clusters 1 and 2 appeared around the pycnocline layer (around the chl *a* maximum layer) and surface layer before the SWE, respectively. Cluster 1 expanded its

distribution to the upper layer and replaced cluster 2. Cluster 3 was found in the lower layer throughout the FPO term. We inferred major phytoplankton taxonomic groups for each

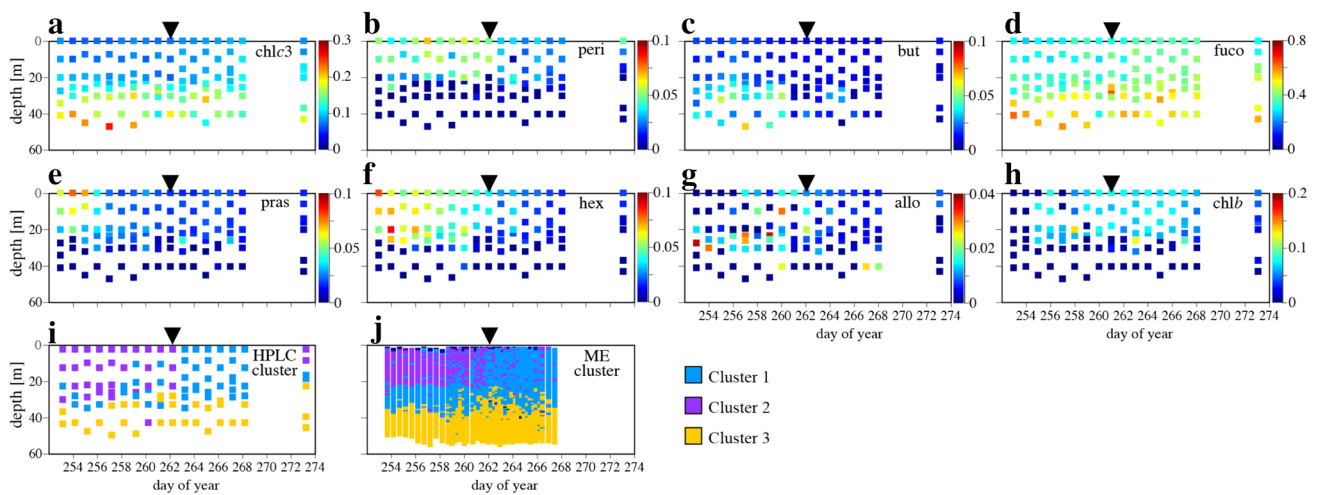


Fig. 4 Time series of vertical distribution of ratios of **a** chlc3, **b** peri, **c** but, **d** fuco, **e** pras, **f** hex, **g** allo, and **h** chlb against chl_a. Vertical distributions of cluster group divided by **i** in situ pigment/chl_a ratios

(HPLC cluster) and **j** pigment/chl_a ratios predicted by the *Multi-Exciter* instrument (ME cluster) are also shown. Black triangles denote onset of the SWE

cluster using pigment composition and pigment/chl_a ratios fully referring to previous related studies (Hill et al. 2005; Fujiwara et al. 2014). The average algal pigment composition is indicated in Fig. 3b and the mean pigment ratios are listed in Table 1. Fuco dominated all the clusters (fuco/chl_a > 0.3), which is a typical characteristic of the Chukchi shelf during fall that has been reported in earlier studies (e.g., Fujiwara et al. 2014; Coupel et al. 2015). However, there is large diversity in the secondary pigment/chl_a ratio among the cluster groups. The taxonomic interpretations for each cluster are documented as below.

Cluster 1 has the highest chl_a concentration (mean ± standard deviation: 0.667 ± 0.226, n = 45) and the second highest fuco/chl_a ratio (0.391 ± 0.024, n = 45) (Fig. 3b and Table 1). The cluster was found in the chl_a maximum layer (around the pycnocline) before the SWE

and it spread into the upper layer after the SWE. However, the other pigment/chl_a ratios are significantly smaller than cluster 2, suggesting a small contribution from non-diatom cultures. Conversely, both the hex/fuco (0.059 ± 0.039, n = 45) and but/fuco (0.038 ± 0.031, n = 45) ratios show much smaller values than cluster 2. Such low values of the hex/fuco and but/fuco ratios indicate that the fuco of cluster 1 was derived mainly from diatoms (Hill et al. 2005). We determined diatoms with highest biomass group that occupied cluster 1.

Cluster 2 in considered influenced by northern surface water communities because of the high presence of accessory pigments such as but, hex, peri, allo, and fuco. These pigment/chl_a ratios are the highest among the clusters. Although the fuco/chl_a ratio (0.308 ± 0.023, n = 34) is close to that of diatom communities found in

Table 1 Means and standard deviations of pigment/chl_a and pigment/pigment ratios used in this study to infer the phytoplankton community composition of each cluster

Pigment	Cluster 1	Cluster 2	Cluster 3
chl _c 3/chl _a	0.101 ± 0.024	0.081 ± 0.019	0.163 ± 0.037
[chl _c 1 + c ₂ + MgDVP]/chl _a	0.129 ± 0.019	0.134 ± 0.012	0.177 ± 0.027
peri/chl _a	0.020 ± 0.014	0.033 ± 0.023	0.000 ± 0.000
but/chl _a	0.015 ± 0.013	0.020 ± 0.009	0.019 ± 0.016
fuco/chl _a	0.391 ± 0.024	0.308 ± 0.023	0.518 ± 0.049
pras/chl _a	0.018 ± 0.007	0.029 ± 0.019	0.002 ± 0.003
hex/chl _a	0.022 ± 0.015	0.049 ± 0.019	0.002 ± 0.004
allo/chl _a	0.006 ± 0.006	0.012 ± 0.011	0.003 ± 0.006
zea/chl _a	0.000 ± 0.000	0.000 ± 0.001	0.000 ± 0.001
lut/chl _a	0.000 ± 0.000	0.000 ± 0.001	0.000 ± 0.001
chl _b /chl _a	0.051 ± 0.032	0.045 ± 0.031	0.003 ± 0.006
hex/fuco	0.059 ± 0.039	0.160 ± 0.062	0.004 ± 0.009
but/fuco	0.038 ± 0.031	0.064 ± 0.027	0.036 ± 0.030

the earlier CHEMTAX (CHEMical TAXonomy) studies in the Arctic seas (Vidussi et al. 2004; Coupel et al. 2015), the highest hex/fuco (0.160 ± 0.062 , $n = 34$) and but/fuco (0.064 ± 0.027 , $n = 34$) ratios reveals that fuco could somehow be attributed to haptophytes. The highest peri/chla (0.033 ± 0.023 , $n = 34$), pras/chla (0.029 ± 0.019 , $n = 34$), and hex/chla (0.049 ± 0.019 , $n = 34$) ratios indicate some fractions of dinoflagellates, prasinophytes, and hex-containing haptophytes next to the diatoms in this cluster, indicative of the highest taxonomic diversity of the clusters.

Cluster 3 shows the highest fuco/chla ratio (0.518 ± 0.049 , $n = 31$) but the lowest chla (0.411 ± 0.533 , $n = 31$) of all the clusters. Pigment/chla ratios are absent or extremely low, except diatom-related pigments (chl*c*3, chl*c*1 + *c*2 + MgDVP, fuco) and the but/fuco ratio. This cluster showed very small temporal and vertical change in its distribution and it was located below the pycnocline throughout the FPO term. Because the cluster is adapted to low chla and high nutrient concentration, we assumed that the growth of phytoplankton assemblages in cluster 3 was strongly light limited. Therefore, we suggest that less productive senescent diatoms mostly contribute to this cluster. Unlike the general pigment composition of this cluster (i.e., high fuco/chla and low chla), we should also note that some of the highest values of chla (> 1.0) observed during the FPO belonged to this group (Fig. 3b). A few samples attributed to this group appeared sporadically around the pycnocline with the water column chla maximum depth (261–262, Julian day, Fig. 4i), i.e., the diatoms with high chla have similar pigment composition to the less productive communities of the lower layer.

Relationship between the cluster group and environmental variables

PCA was applied to the environmental variables (temperature, salinity, %PAR relative to surface value, TIN, phosphate, silicate, f_{SIM} , and f_{OF}) to enable the visualization of the similarities and differences of the environmental conditions. PC1 and PC2 explained 64 and 17% of the vertical and temporal environmental variability, respectively. A scatter plot of PC1 and PC2 colored by the cluster groups of pigment composition is shown in Fig. 5. It is helpful to understand the relationship between the suitable habitat for the clustered phytoplankton communities and the environmental conditions, as well as the vertical and temporal variations of the environmental variables. PC1 was determined principally by temperature and salinity, which almost explains the vertical features of the environmental variables. The other environmental characteristics modified by the SWE are represented by PC2. Warm, fresh, and oligotrophic surface water at the beginning of the FPO term was occupied by cluster 2 ($PC1 = -4$ to -2 and $PC2 = -3$ to -1).

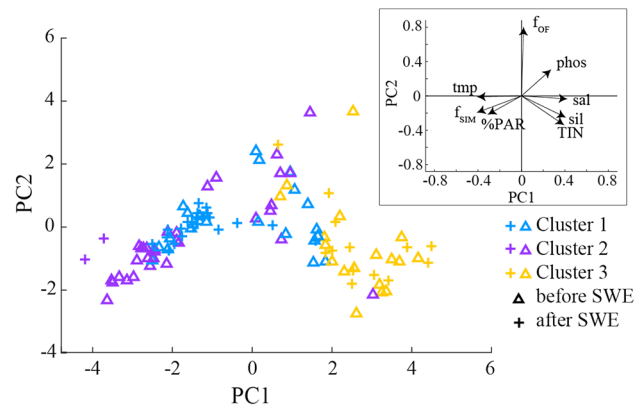


Fig. 5 Result of principal component analysis (PCA) for the environmental variables where HPLC data were collected. The variance in the data was majorly explained by principal component 1 (PC1) (64.3%) and component 2 (PC2) (17.2%). Plots are distinguished according to the clustered group and sampled timing; crosses and triangles denote samples taken before and after the SWE, respectively. The vectors of loadings are also shown in the discrete panel; *tmp* temperature, *sal* salinity, *TIN* total inorganic nitrogen concentration, *phos* phosphate concentration, *sil* silicate concentration, %PAR percent PAR relative to surface PAR, f_{SIM} fraction of sea ice melt water, f_{OF} fraction of other fresh water

Cluster 1 first appeared at intermediate depth with moderate nutrient conditions where a subsurface f_{OF} maximum occurred ($PC1 = 0$ – 2 and $PC2 = 0$ – 3). However, its distribution expanded to the surface along with the nutrient supply after the occurrence of the SWE ($PC1 = -3$ to -1 and $PC2 = -2$ to 1). Cluster 2 was suited largely to the less saline, high temperature, and low nutrient conditions of the upper layer ($PC1 < -2$, $PC2 < 0$), but it disappeared after the SWE. Cluster 3 was distributed mainly in the cold, saline, high nutrient, and low irradiance conditions of the bottom layer ($PC1 > 2$ and $PC2 = -2$ to 2). However, as noted in “Inference of taxonomic composition” section, cluster 3 also appeared with high chla (> 1.0) with similar pigment composition to the lower community, which is plotted in the range of $PC1 < 2$ and $PC2 > 0$.

Interpretation of pigment/chla ratio using the Multi-Exciter

The EOF analysis of the standardized excitation spectra indicated that the first five modes explained 88.7, 8.29, 1.71, 0.58, and 0.34% of the spectral variance, respectively, i.e., their cumulative contribution accounted for 99.62%. Then, we selected the target pigments (chl*c*3, peri, but, fuco, pras, hex, allo, and chl*b*) that were used for the cluster analysis (see “Inference of taxonomic compositions” section) for the prediction. Because the accessory pigment/chla ratios had a lower limit of 0 and would never exceed 1, we chose a

sigmoidal model to represent the variation of the pigment/chla ratios:

$$\text{Pigment/chla} = 1 / (1 + \exp(-(\beta_0 + \beta_1 S_1 + \beta_2 S_2 + \beta_3 S_3 + \beta_4 S_4 + \beta_5 S_5))), \tag{1}$$

where S_{1-5} are the EOF scores and β_{0-5} are the partial regression coefficients listed in Table 2. Thus, the pigment/chla ratios could be derived from Eq. 1. The comparisons and statistics of the modeled and in situ pigment/chla ratios are shown in Fig. 6. The root mean square errors (RMSEs) and determination coefficients between the modeled and in situ pigment/chla ratios are also listed (Table 2). The RMSEs range between 0.007 and 0.020, and the values of r^2 exceed 0.5 in all focused pigment/chla ratios except allo ($r^2 = 0.05$).

The *Multi-Exciter* was also used to assess the short-term changes in phytoplankton community composition with high temporal and vertical resolutions. The EOF scores

S_n ($n = 1-5$) for unknown samples were reconstructed as below:

$$S_n = (z(\lambda) - \mu(\lambda)) / l_n(\lambda), \tag{2}$$

where $z(\lambda)$, $\mu(\lambda)$, and $l_n(\lambda)$ are the standardized fluorescence value, estimated mean value of $z(\lambda)$, and loadings of EOF mode n for each wavelength λ , respectively. The values of $\mu(\lambda)$ and $l_n(\lambda)$ are listed in Table 3. The time series of the clustered phytoplankton groups predicted by the *Multi-Exciter* for the FPO site is shown in Fig. 4j. The vertical and temporal distributions of the clustered groups at the FPO site match the groups predicted from in situ pigment ratios well (Fig. 4i, j).

To evaluate the spatial generality of the response of phytoplankton community structure to the SWE, we investigated the time series of the environmental variables (Fig. 7) and pigment/chla ratios at the four sub-FPO stations (A, B, C, and D) (Fig. 8). Atmospheric and CTD observations without water sampling captured the

Table 2 Regression coefficients for Eq. (1)

	chl _c 3	peri	but	fuco	pras	hex	allo	chl _b
β_0	-2.121	-5.296	-4.040	-0.422	-4.596	-4.039	-5.041	-4.225
β_1	-0.318	2.700	-0.317	-0.233	1.414	1.241	0.546	2.503
β_2	-0.565	2.044	0.714	-0.676	1.781	1.500	n.s.	n.s.
β_3	-0.875	-1.001	-1.499	n.s.	-1.304	n.s.	-3.278	-3.095
β_4	-1.733	6.717	n.s.	-1.255	1.854	1.731	n.s.	4.015
β_5	-0.979	8.119	-5.739	n.s.	-2.601	-5.154	n.s.	n.s.
r^2	0.74	0.72	0.63	0.67	0.71	0.74	0.05	0.54
RMSE	0.023	0.010	0.008	0.051	0.008	0.012	0.007	0.018

Coefficients that satisfied $p < 0.05$ (t test) were selected. n.s. denotes no significant coefficient was obtained. r^2 and RMSE between in situ and predicted pigment/chla ratio are also provided

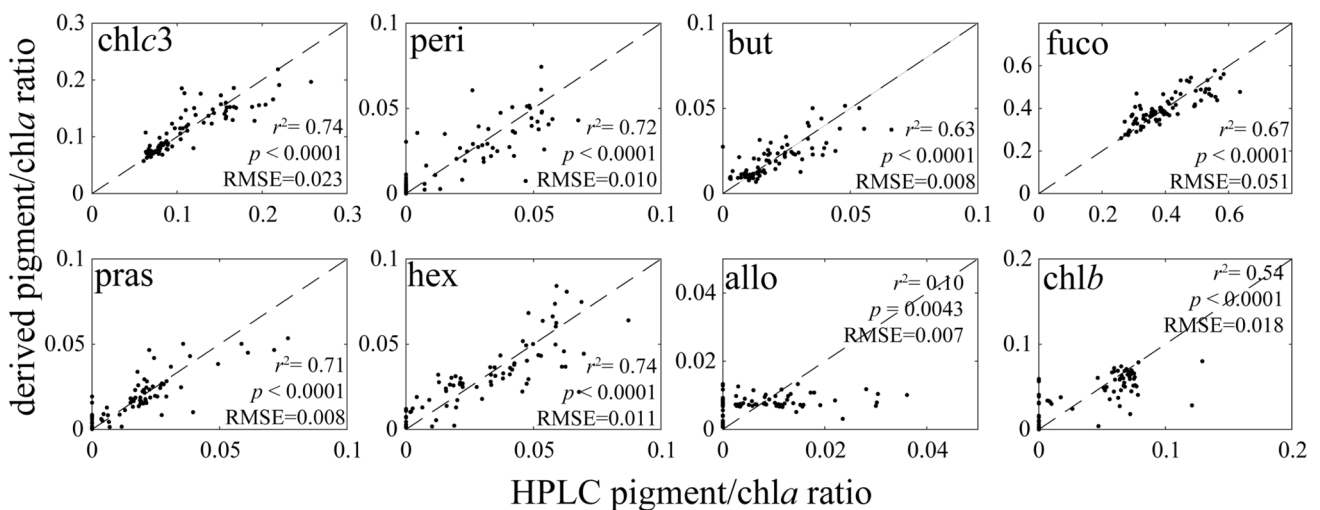


Fig. 6 Comparison of HPLC measured and *Multi-Exciter* predicted ratios of chl_c3, peri, but, fuco, pras, hex, allo, and chl_b against chl_a. Dashed lines indicate 1:1 line. Statistics between HPLC and reconstructed pigment/chla ratios are also shown in Table 2

Table 3 Loadings of the 1st to 5th EOF mode (l_{1-5}) and estimated mean of standardized fluorescence value (μ) for the *Multi-Exciter* measured wavelengths (λ)

λ (nm)	l_1	l_2	l_3	l_4	l_5	μ
375	-0.371	-0.190	-0.258	-0.106	-0.430	-0.106
400	-0.531	-0.159	-0.285	-0.155	-0.032	0.319
420	-0.190	0.029	-0.183	0.294	0.632	0.887
435	0.289	0.083	-0.236	0.587	0.082	1.205
470	0.656	-0.086	-0.423	-0.303	-0.213	1.153
505	0.117	-0.138	0.235	-0.078	0.141	-0.725
525	0.116	-0.498	0.534	-0.252	0.230	-1.164
570	-0.046	0.793	0.144	-0.426	0.116	-0.448
590	-0.040	0.167	0.472	0.438	-0.526	-1.120

SWE, and water convection was found to have occurred homogeneously at all the stations; however, the initial conditions were slightly different. The vertical water mass structure at the near-shelf break sites (FPO, stations A and B) (Figs. 2b, c, 7b, c, e, f) was similar, but rather weaker stratification and a shallower surface mixed layer depth were found at shelf side sites (stations C and D) (Fig. 7 h, i, k, l). The predicted pigment/chl*a* ratios followed the physical structure; a smaller fraction of fuco/chl*a* ratio was found at the FPO site (Fig. 2d) and at stations A and B (Fig. 8a, d) before the SWE compared with stations C and D (Fig. 8g, j). Since the observation sites were set at the edge of the shelf region, initial physical and biological condition showed a weak gradient from shelf to shelf break area. However, the SWE seems to have mixed the upper layer homogeneously throughout the region and thus,

the temperature decrease and salinity increase were found at all stations (Fig. 7). The fuco/chl*a* ratio also increased at all stations but conversely, the hex/chl*a* and pras/chl*a* ratios decreased significantly (Fig. 8). It is notable that low salinity water (< 31.5), probably warmed SIMW (Fig. 2j), appeared suddenly in the upper layer at station C during 263–265 (Julian day) with a slightly lower temperature (~ 1 °C) (Fig. 7h, i). A slightly higher hex/chl*a* and pras/chl*a* ratios co-occurred with this peculiar water mass (Fig. 8h, i).

Change in grazing rate of *Calanus glacialis* C5

The grazing rates of *C. glacialis* on different size phytoplankton before and after the SWE are compared in Fig. 9. The grazing rates were nearly zero on all size classes before

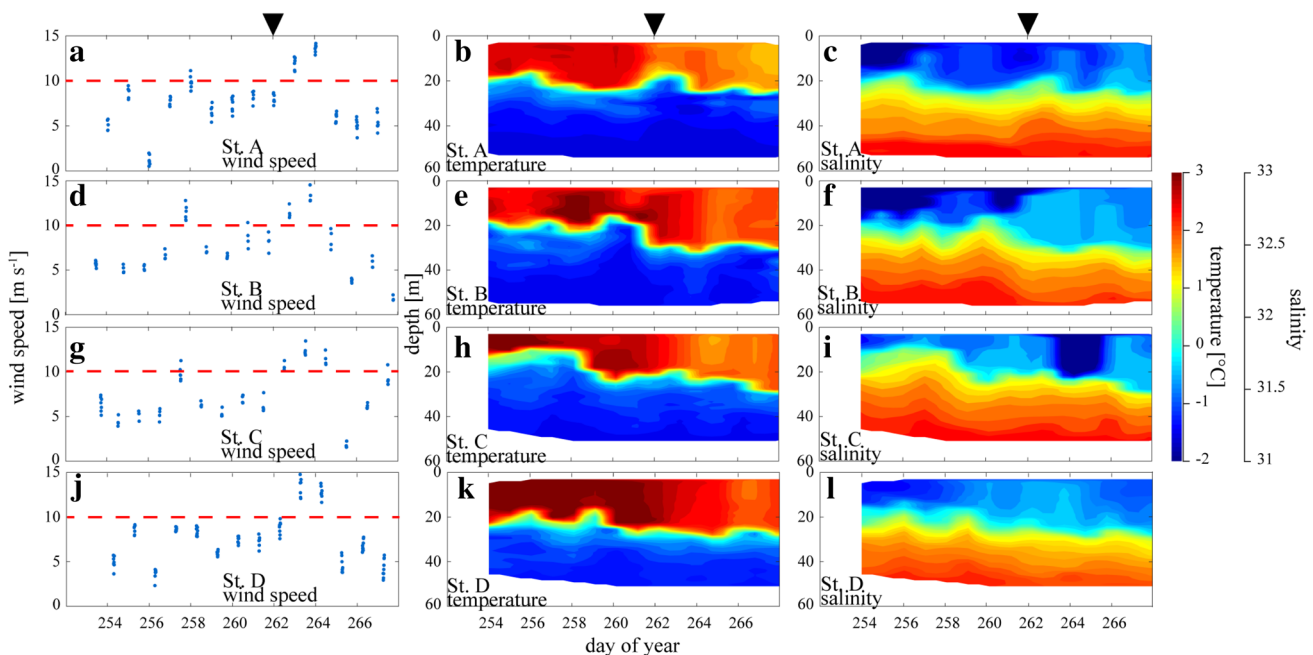


Fig. 7 Time series of wind speed (left panels, a, d, g, j), temperature (center panels, b, e, h, k), and salinity (right panels, c, f, i, l) for the sub-FPO stations (A, B, C, and D). Red solid lines in the panels of wind speed indicate 10 m s⁻¹ and black triangles represent the onset of the SWE

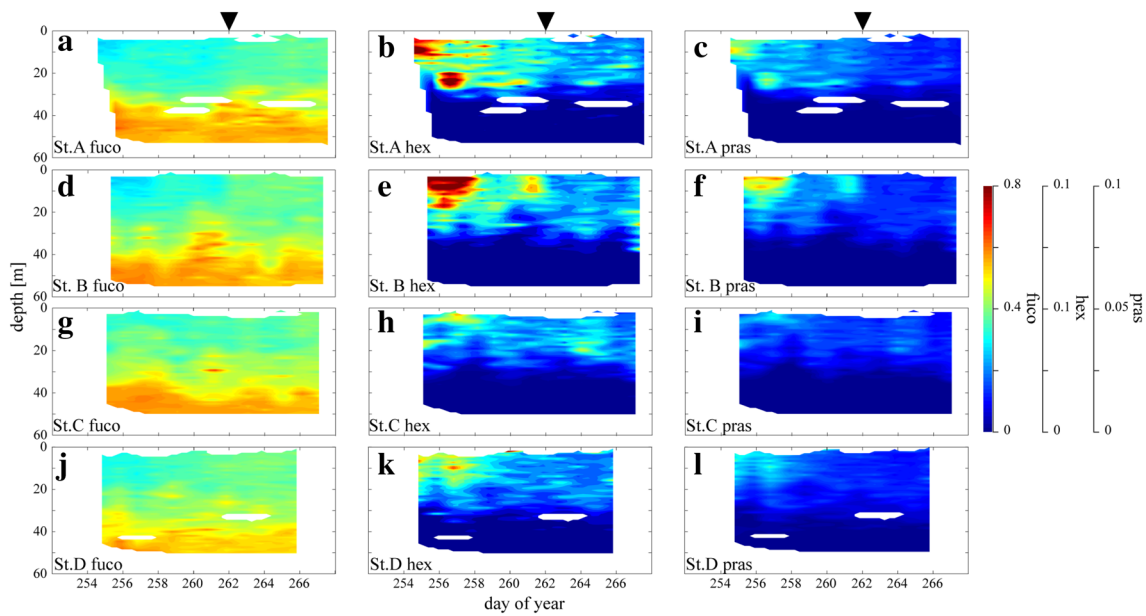


Fig. 8 Fuco/*chl a* (left panels, **a, d, g, j**), hex/*chl a* (center panels, **b, e, h, k**), and pras/*chl a* (right panels, **c, f, i, l**) for the sub-FPO stations (A, B, C, and D). Black triangles represent the onset of the SWE

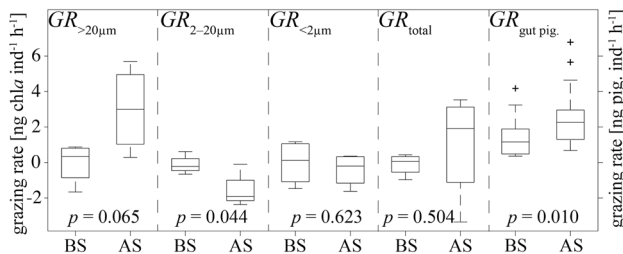


Fig. 9 Comparison of grazing rate of *Calanus glacialis* C5 before (BS) and after the SWE (AS). Grazing rates were calculated for *chl a* attributed to microphytoplankton ($GR_{>20\mu m}$), nanophytoplankton ($GR_{2-20\mu m}$), picophytoplankton ($GR_{<2\mu m}$), and total phytoplankton (GR_{total}). Grazing rate calculated by gut pigment (Matsuno et al. 2015) is also provided for comparison ($GR_{gut\ pig.}$) with right axis. The boxplots indicate values of median (horizontal bars), 25 and 75% quartiles (box ranges), confident intervals (whiskers), and outliers (crosses). Statistical differences between grazing rates before and after the SWE are shown (*p*-values, *U* test)

the SWE. Remarkable but different responses were found among the various sizes after the SWE. The most significant change in grazing rate was found on nanophytoplankton ($chl a_{2-20\mu m}$). The median grazing rate on nanophytoplankton decreased from -0.22 to -1.92 ng *chl a* ind⁻¹ h⁻¹ (*U* test, *p* = 0.044). The second largest change was found in $chl a_{>20\mu m}$, which showed a gradual increase in median value from 0.33 to 2.99 ng *chl a* ind⁻¹ h⁻¹ (*U* test, *p* = 0.065). However, there were no significant changes in grazing rates on picophytoplankton ($chl a_{<2\mu m}$) and total *chl a* ($chl a_{total}$). For comparison, the grazing rate measured by Matsuno et al.

(2015) using the gut pigment method is also illustrated in Fig. 9. It shows a very similar response in grazing rate on microphytoplankton, with a significant increase after the SWE (from 1.16 to 2.27 ng pigment ind⁻¹ h⁻¹, *U* test, *p* = 0.010).

Discussion

Interpretation of taxonomic composition using HPLC pigments

Pigment signatures have been used widely to infer the vertical and horizontal distributions of phytoplankton taxonomic groups at the class level in the western Arctic Ocean (Hill et al. 2005; Coupel et al. 2012, 2015; Fujiwara et al. 2014). Several methods exist for the interpretation of phytoplankton groups from accessory pigment concentrations, e.g., multiple regression analysis and the CHEMTAX method (Wright and Jeffrey 2006). The multiple regression method quantifies the contribution of accessory pigments toward *chl a* using several accessory pigments. It is suitable for data where the taxonomic composition is unknown (Wright and Jeffrey 2006). However, we were unable to obtain the proper equation (not shown). Only few pigments showed statistically significant coefficients, which could be attributed to the narrow range of *chl a* variation during the FPO term. Thus, a larger range of *chl a* variation is required for proper *chl a* quantification using accessory pigments. On the other hand, the CHEMTAX method is not restricted by *chl a* range

and it is suitable for the detection of the *chl a* contributions of even minor pigments (Mackey et al. 1996). However, CHEMTAX is sensitive to the initial specific pigment/*chl a* ratios for the target taxa, which vary largely with region and season, and they have not yet been established for our study area. In addition, because we unfortunately did not conduct microscopic analysis for the detailed identification of phytoplankton species, target taxa are difficult to determine and validate. For these reasons, the taxonomic composition was inferred from the patterns of pigment composition fully referring to previous studies of Arctic waters (e.g., Booth and Horner 1997; Vidussi et al. 2004; Hill et al. 2005; Sukhanova et al. 2009; Joo et al. 2012; Coupel et al. 2012, 2015; Fujiwara et al. 2014).

Short-term changes of phytoplankton community structure

Before the SWE, the water column structure of the FPO sites exhibited typical stratified two-layered condition, i.e., a large fraction of warmed sea ice meltwater in the upper layer and saline Pacific winter water in the lower layer. The strong stratification of the water column meant that nutrients were almost depleted in the top layer consequence of primary production after the sea ice melt. The SWE enhanced internal waves and wind-induced mixing, which weakened the stratification (Kawaguchi et al. 2015; Nishino et al. 2015). The upper layer mixing and subsequent nutrient supply from lower layer enhanced surface *chl a* from 0.33 to 0.84 $\mu\text{g L}^{-1}$ in average. Such magnitude of surface *chl a* is not normally seen around the FPO site from the satellite observation (Fig. 1a). Although we acquired 35 scenes of satellite *chl a* during Septembers of 2003–2015, we found that only the 4 scenes exceeded 0.8 $\mu\text{g L}^{-1}$ (Fig. 1b). Therefore, it can be said that the fall bloom in the shelf region of the central Chukchi Sea is an episodic event.

During the FPO term, fuco/*chl a* ratios were always higher than other pigment/*chl a* ratios. This characteristic is widely observed in the surface layer of the shelf region during fall (Fujiwara et al. 2014). Coupel et al. (2012) also reported that the contribution of fuco to total accessory pigments exceeded 70% on the Chukchi shelf during summer. Although fuco is commonly used as a proxy of diatom pigment (e.g., Jeffrey and Vesk 1997), microscopic analysis suggests that fuco in the surface layer of the Chukchi shelf and Canada Basin originates from nanophytoplankton. During the FPO term, Nishino et al. (2015) reported that small phytoplankton ($< 20 \mu\text{m}$) was predominant in the upper layer before the SWE. Our data revealed hex, pras, and peri ratios against *chl a* were larger before the SWE in the upper layer where a relatively large value of f_{SIM} was found. Such a large value of f_{SIM} is typical of the surface water

of the northern basin area during late summer to fall (e.g., Yamamoto-Kawai et al. 2005) where non-diatom communities such as prasinophytes, green-algae, and haptophytes are generally predominant (Hill et al. 2005; Sukhanova et al. 2009; Joo et al. 2012; Coupel et al. 2012; Fujiwara et al. 2014). In such waters, nutrients are generally depleted and small-celled phytoplankton and regenerated production are common (e.g., Sherr et al. 2003; Hill et al. 2005; Matsuno et al. 2014). Community structures for the subsurface *chl a* maximum were also reported and generally pennate and centric diatoms were predominant in terms of cell abundance or *chl a* concentration (Sukhanova et al. 2009; Joo et al. 2012; Coupel et al. 2012). Consistent with these past studies, a higher fuco/*chl a* ratio was found at the depth of *chl a* maximum during the FPO term, which increased after the SWE. An increase in the *chl a* and fuco/*chl a* ratio in the upper layer was probably attributed to the remarkable increase in the pennate diatom *Cylindrotheca closterium* (Yokoi et al. 2016). The replacement of the algal community of cluster 2 by cluster 1 in the upper layer could be the consequence of changes in pigment composition with pulsed production of pennate diatoms. Such a dramatic increase in pennate diatoms is likely to have contributed to the doubling of the water column primary production (Nishino et al. 2015). These results also suggest that the phytoplankton community in the subsurface *chl a* maximum plays an important role for the development of the fall bloom phytoplankton owing to increased light and nutrient availability via the wind-induced mixing.

The relationships between the environmental variables and phytoplankton community structures are visualized well by the PCA plot (Fig. 5). Suitable environmental conditions for each clustered group can be explained approximately by PC1; clusters 1, 2, and 3 are adapted to small, moderate, and large PC1, respectively. In contrast, PC2 can be treated as the proxy of pycnocline strength, where the f_{OF} maximum occurs (Nishino et al. 2015). The homogenization of water properties in the upper layer by the SWE reduced PC2, i.e., the stratification weakened and cluster 2 disappeared after the SWE. Such replacement of the upper layer community of cluster 2 by cluster 1 can be explained by the positive and negative contributions of phosphate and f_{SIM} . However, TIN and silicate apparently showed very weak contributions to the taxonomic changes in the upper layer. Because of the immediate use of TIN for primary production (Nishino et al. 2015), TIN supply from the lower layer was difficult to detect. This is why TIN and silicate showed much weaker contributions to the switching of the surface phytoplankton community. Overall, the PCA revealed that temporal changes in the phytoplankton community structure were concomitant with environmental variations.

Interpretation of phytoplankton groups using *Multi-Exciter*

Measurement of multi-spectral excitation/emission fluorescence is a rapid and costless method for the determination of phytoplankton taxonomic composition (MacIntyre et al. 2010). However, it requires suitable calibration of pigment–taxonomy relationships using pure cultures of the target species. The *Multi-Exciter* also requires pre- or post-calibration using the spectral fluorescence features of pure culture samples of the target species (Yoshida et al. 2011). During field sampling, it is difficult to predict those types of species that will appear at the observation site. In the case of the western Arctic Ocean, several past studies have already reported the relationship between taxonomy and pigment composition (Hill et al. 2005; Coupel et al. 2012, 2015). Therefore, the derivation of pigment/*chl a* ratio using the *Multi-Exciter* could provide important information for inferring and monitoring phytoplankton communities in the western Arctic Ocean.

The relationships between in situ and predicted pigment/*chl a* ratios showed good agreement except for *allo* and *chl b* (Fig. 6, Table 2). We should note that the pigments that appear constantly, such as *fuco*, *but*, and *pras*, are better predicted than those that appear sporadically, such as *allo* and *chl b*. Despite the poorer predictions of *chl b/chl a* and *allo/chl a* ratios, the cluster analysis applied to the *Multi-Exciter*-predicted pigment/*chl a* ratios also showed good agreement with the in situ clustered groups, in both their vertical and their temporal patterns (Fig. 4i, j); the timing of the switching of surface communities and vertical locations of the clusters were well matched. This is because *allo* is one of the major accessory pigments that contribute to *chl a* variability. However, the *allo/chl a* ratio was quite low (~ 0.03 maximum) compared with other pigments and thus, it did not have much effect on the clustering result. Our results reveal that interpolative use of the *Multi-Exciter* for the monitoring of phytoplankton pigment is practical for high-resolution observation. Unfortunately, we did not obtain samples independent of the model development data for the validation of the model; however, such matching of the distribution patterns in cluster groups supports proper use of the model. Moreover, as shown in Fig. 8, every 24 h observation using the *Multi-Exciter* at the stations 16 km from the FPO site also showed significant responses in pigment signatures to the SWE and subsequent environmental changes. That is, the initial oceanic conditions at the FPO and sub-FPO sites were different, though changes in phytoplankton community structure occurred at the four other stations as well as at the FPO site. It suggests that such extrapolative use to confirm the spatial generality of phytoplankton response to environmental forcing is also practical. Therefore, we would like to highlight that the prediction of pigment/*chl a* ratios using the

Multi-Exciter with in situ optimization is applicable for the high-frequency observations and for inferring phytoplankton community structure. Recently published analysis using the *Multi-Exciter* has also demonstrated the effectiveness of in situ optimization using CHEMTAX-derived taxa in the East China Sea (Wang et al. 2016). It is expected to advance our knowledge of the variability of the temporal and spatial distributions of phytoplankton assemblages by attachment to CTD profilers, moorings, or by application to continuous monitoring of surface water.

Response of grazing rate of *Calanus glacialis* C5

Calanoid copepods comprised 60% of the total zooplankton abundance during the FPO term. *Pseudocalanus* spp. and *C. glacialis* were the dominant species of zooplankton (Matsuno et al. 2015), accounting for 60 and 35% of the total copepod abundance, respectively. Considering its large body size and biomass, *C. glacialis* is considered a key species in the waters of the Arctic shelves (Conover and Huntley 1991; Lane et al. 2008). It is important to assess their response of feeding activity to the eventual fall bloom. Matsuno et al. (2015) has reported a temporal change in grazing rate and grazing impact of *C. glacialis* C5 during the FPO using the gut pigment approach. They showed that the grazing rate increased significantly with *chl a* after the SWE (from 0.11 to 0.18 ng pigment ind⁻¹ day⁻¹). In addition to their study, we measured the grazing rate of *C. glacialis* C5 for three size classes of phytoplankton using the incubation approach. Our results revealed an increase of grazing rate on microphytoplankton (> 20 µm) after the SWE that was consistent with the gut pigment approach. Another notable point is that the grazing rate for nanophytoplankton showed negative values and a significant decrease after the SWE. A similar phenomenon for nanophytoplankton was reported in another region under grazing experiment conditions of copepods with incubation bottles. For example, Liu and Dagg (2003) reported *chl a* of sizes < 5 µm or 5–20 µm increased after adding mesozooplankton, suggesting that mesozooplankton grazing caused the removal of microzooplankton, which reduced the grazing pressure on small phytoplankton. Similarly, selective grazing of *Neocalanus* spp. on larger particles in the Pacific Ocean has been found to enhance smaller phytoplankton growth in the incubation environment through the cascade effect (Liu et al. 2005; Dagg et al. 2006, 2009). In the study region, Campbell et al. (2009) reported strong food preference of *C. glacialis* for microzooplankton rather than diatoms because of the decline of food quality of the diatoms in post-bloom conditions. Although we did not measure the grazing rate of microzooplankton, a decrease in the grazing rate on nanophytoplankton after the SWE is believed to result from reduced microzooplankton grazing pressure. We also would like to note that grazing rates on

all size classes of phytoplankton were nearly zero before the SWE, indicating the minimal cascade effect and minimal feeding activity of *C. glacialis* on both microzooplankton and microphytoplankton. This might be because *C. glacialis* prepared for diapause (Matsuno et al. 2015). However, the fall bloom apparently enhanced the feeding activity of *C. glacialis* not only on microphytoplankton but also on microzooplankton. Estimated food requirements of *C. glacialis* C5 during the FPO term suggest that the enhanced phytoplankton biomass is still insufficient to maintain their population and thus, another food source was suggested by Matsuno et al. (2015) The significant cascade effect found in this study supported their suggestion that microzooplankton is likely consumed by *C. glacialis* C5 together with increased quantities of microphytoplankton.

We captured the enhanced diatom biomass that is clearly transferred to *C. glacialis*, which is the key species linking the primary producers and higher trophic level organisms in the waters of the Arctic shelves (Søreide et al. 2010). However, it is still unknown whether the fall bloom positively affects their life cycle. It seems that the fall bloom can provide additional energy for secondary producers before overwintering. Seasonal succession of phytoplankton species is reported to have large impact on secondary producers. For example, Leu et al. (2011) reported that yearly changes in the seasonal succession of ice algae and phytoplankton cause yearly differences in *C. glacialis* recruitment and reproduction in the Rijpfjorden (European Arctic shelf). In the Beaufort Sea, episodic fall blooms have obvious impact on the recruitment of secondary producers (Tremblay et al. 2011). Similarly, yearly changes in the timing of the spring bloom have significant impact on the production of higher trophic level organisms through the food web in the Bering Sea (reviewed in Hunt et al. 2002, 2011). The impact on secondary producers as a whole remains unknown because the grazing experiments were conducted only for *C. glacialis* C5, even though they comprise one-third of the total mesozooplankton abundance. As secondary producers can be sensitive to changes in primary producers, further research is required to comprehend the roles of fall blooms in the entire ecosystem with reference to the recent increase in the number of stormy days during fall in the Chukchi Sea (e.g., Serreze et al. 2000; Zhang et al. 2004; Sepp and Jaagus 2011).

Summary and conclusions

HPLC pigment signatures clearly captured the changes in phytoplankton community structure with environmental changes triggered by the SWE that occurred during the FPO term. The SWE was sufficiently strong to supply nutrients from the lower layer to the upper layer and to enhance diatom biomass, which was severely nitrate-limited during

the post-bloom conditions. We developed a model to enable high-frequency measurements of the pigment signature from multi-wavelength excitation/emission fluorescence spectra by quantifying the relationship between in situ pigment concentrations and excitation spectra. The changes in phytoplankton pigment signature were also observed by *Multi-Exciter*. Moreover, the grazing experiment of *C. glacialis* C5 revealed a significant increase of feeding activity, supporting potential increased consumption of diatoms together with microzooplankton, which could affect the success of overwintering and reproduction in the following spring. Thus, the SWEs on the Chukchi shelf during fall have remarkable impact on both primary and secondary producers (Matsuno et al. 2015; Yokoi et al. 2016). The occurrence of the fall bloom, or changes in its magnitude and timing, is noteworthy to comprehend the recent drastic ecosystem changes in the Arctic Ocean.

Acknowledgements We thank the captain, officers, and crews of the *R/V Mirai*. We also appreciate the staff of Marine Works Japan Ltd. and Global Ocean Development, Inc. for their skillful samplings and analysis of the data. This research was funded by the Japan Society for the Promotion of Science (JSPS) (KAKENHI, 7112771), GRENE Arctic Climate Change Research Project, and Arctic Challenge for Sustainability (ArCS) Project.

Open Access This article is distributed under the terms of the Creative Commons Attribution 4.0 International License (<http://creativecommons.org/licenses/by/4.0/>), which permits unrestricted use, distribution, and reproduction in any medium, provided you give appropriate credit to the original author(s) and the source, provide a link to the Creative Commons license, and indicate if changes were made.

References

- Alou-Font E, Mundy CJ, Roy S et al (2013) Snow cover affects ice algal pigment composition in the coastal Arctic Ocean during spring. *Mar Ecol Prog Ser* 474:89–104
- Aoyama M, Hydes DJ (2010) How do we improve the comparability of nutrient measurements? In: Aoyama M, Dickson AG, Hydes DJ, Murata A, Oh JR, Roose P, Woodward EMS (eds) Comparability of nutrients in the world's ocean. Mother Tank, Tsukuba, pp 1–10
- Ardyna M, Gosselin M, Michel C et al (2011) Environmental forcing of phytoplankton community structure and function in the Canadian High Arctic: contrasting oligotrophic and eutrophic regions. *Mar Ecol Prog Ser* 442:37–57. <https://doi.org/10.3354/meps09378>
- Ardyna M, Babin M, Gosselin M et al (2014) Recent Arctic Ocean sea ice loss triggers novel fall phytoplankton blooms. *Geophys Res Lett*. <https://doi.org/10.1002/2014GL061047>
- Booth BC, Horner RA (1997) Microalgae on the arctic ocean section, 1994: species abundance and biomass. *Deep-Sea Res II* 44:1607–1622. [https://doi.org/10.1016/S0967-0645\(97\)00057-X](https://doi.org/10.1016/S0967-0645(97)00057-X)
- Bopp L, Aumont O, Belviso S, Monfray P (2003) Potential impact of climate change on marine dimethyl sulfide emissions. *Tellus B* 55:11–22
- Bracher A, Taylor MH, Taylor B et al (2015) Using empirical orthogonal functions derived from remote-sensing reflectance for the

- prediction of phytoplankton pigment concentrations. *Ocean Sci* 11:139–158. <https://doi.org/10.5194/os-11-139-2015>
- Caliński T, Harabasz J (1974) A dendrite method for cluster analysis. *Commun Stat* 3:1–27. <https://doi.org/10.1080/03610927408827101>
- Campbell R, Sherr E, Ashjian C et al (2009) Mesozooplankton prey preference and grazing impact in the Western Arctic Ocean. *Deep-Sea Res II* 56:1274–1289
- Comiso JC, Parkinson CL, Gersten R, Stock L (2008) Accelerated decline in the Arctic sea ice cover. *Geophys Res Lett* 35:L01703. <https://doi.org/10.1029/2007GL031972>
- Conover R, Huntley M (1991) Copepods in ice-covered seas—distribution, adaptations to seasonally limited food, metabolism, growth patterns and life cycle strategies in polar seas. *J Mar Syst* 2:1–41. [https://doi.org/10.1016/0924-7963\(91\)90011-1](https://doi.org/10.1016/0924-7963(91)90011-1)
- Cota GF, Wang J, Comiso JC (2004) Transformation of global satellite chlorophyll retrievals with a regionally tuned algorithm. *Remote Sens Environ* 90:373–377. <https://doi.org/10.1016/j.rse.2004.01.005>
- Coupe P, Jin HY, Joo M et al (2012) Phytoplankton distribution in unusually low sea ice cover over the Pacific Arctic. *Biogeosciences* 9:4835–4850. <https://doi.org/10.5194/bg-9-4835-2012>
- Coupe P, Matsuoka A, Ruiz-Pino D et al (2015) Pigment signatures of phytoplankton communities in the Beaufort Sea. *Biogeosciences* 12:991–1006. <https://doi.org/10.5194/bg-12-991-2015>
- Coyle KO, Eisner LB, Mueter FJ et al (2011) Climate change in the southeastern Bering Sea: impacts on pollock stocks and implications for the oscillating control hypothesis. *Fish Oceanogr* 20:139–156. <https://doi.org/10.1111/j.1365-2419.2011.00574.x>
- Craig SE, Jones CT, Li WKW et al (2012) Deriving optical metrics of coastal phytoplankton biomass from ocean colour. *Remote Sens Environ* 119:72–83. <https://doi.org/10.1016/j.rse.2011.12.007>
- Cushing DH (1989) A difference in structure between ecosystems in strongly stratified waters and in those that are only weakly stratified. *J Plankton Res* 11:1–13. <https://doi.org/10.1093/plankt/11.1.1>
- Dagg MJ, Liu H, Thomas AC (2006) Effects of mesoscale phytoplankton variability on the copepods *Neocalanus flemingeri* and *N. plumchrus* in the coastal Gulf of Alaska. *Deep-Sea Res I* 53:321–332. <https://doi.org/10.1016/j.dsr.2005.09.013>
- Dagg M, Strom S, Liu H (2009) High feeding rates on large particles by *Neocalanus flemingeri* and *N. plumchrus*, and consequences for phytoplankton community structure in the subarctic Pacific Ocean. *Deep-Sea Res I* 56:716–726. <https://doi.org/10.1016/j.dsr.2008.12.012>
- Fujiwara A, Hirawake T, Suzuki K et al (2014) Timing of sea ice retreat can alter phytoplankton community structure in the western Arctic Ocean. *Biogeosciences* 11:1705–1716. <https://doi.org/10.5194/bg-11-1705-2014>
- Goés JI, Gomes HDR, Haugen EM et al (2014) Fluorescence, pigment and microscopic characterization of Bering Sea phytoplankton community structure and photosynthetic competency in the presence of a Cold Pool during summer. *Deep-Sea Res II* 109:84–99. <https://doi.org/10.1016/j.dsr2.2013.12.004>
- Grebmeier JM (2012) Shifting Patterns of Life in the Pacific Arctic and Sub-Arctic Seas. *Annu Rev Mar Sci* 4:63–78. <https://doi.org/10.1146/annurev-marine-120710-100926>
- Grebmeier J, Moore S, Overland J (2010) Biological response to recent Pacific Arctic sea ice retreats. *Eos Trans* 91:161–162
- Hill V, Cota G, Stockwell D (2005) Spring and summer phytoplankton communities in the Chukchi and Eastern Beaufort Seas. *Deep-Sea Res II* 52:3369–3385. <https://doi.org/10.1016/j.dsr2.2005.10.010>
- Houliet E, Lizon F, Thyssen M et al (2012) Spectral fluorometric characterization of Haptophyte dynamics using the FluoroProbe: an application in the eastern English Channel for monitoring *Phaeocystis globosa*. *J Plankton Res* 34:136–151. <https://doi.org/10.1093/plankt/fbr091>
- Hunt GL Jr, Stabeno P, Walters G et al (2002) Climate change and control of the southeastern Bering Sea pelagic ecosystem. *Deep-Sea Res II* 49:5821–5853. [https://doi.org/10.1016/S0967-0645\(02\)00321-1](https://doi.org/10.1016/S0967-0645(02)00321-1)
- Hunt GL Jr, Coyle KO, Eisner LB et al (2011) Climate impacts on eastern Bering Sea foodwebs: a synthesis of new data and an assessment of the oscillating control hypothesis. *ICES J Mar Sci* 68:1230–1243. <https://doi.org/10.1093/icesjms/fsr036>
- Hydes DJ, Aoyama M, Aminot A, et al (2010) Determination of dissolved nutrients (N, P, Si) in seawater with high precision and inter-comparability using das-segmented continuous flow analysers. In: Hood EM, Sabine CL, Sloyan BM (eds) *The GO-SHIP repeat hydrography manual: a collection of expert reports and guidelines*, IOCCP report number 14, ICPO publication series number 134, UNESCO-IOC, Paris, France. <http://www.go-ship.org/HydroMan.html>
- Inoue J, Yamazaki A, Ono J et al (2015) Additional Arctic observations improve weather and sea-ice forecasts for the Northern Sea Route. *Sci Rep* 5:16868. <https://doi.org/10.1038/srep16868>
- Isada T, Hirawake T, Kobayashi T et al (2015) Hyperspectral optical discrimination of phytoplankton community structure in Funka Bay and its implications for ocean color remote sensing of diatoms. *Remote Sens Environ* 159:134–151. <https://doi.org/10.1016/j.rse.2014.12.006>
- Itoh M, Pickart RS, Kikuchi T et al (2015) Water properties, heat and volume fluxes of Pacific water in Barrow Canyon during summer 2010. *Deep-Sea Res I* 102:43–54. <https://doi.org/10.1016/j.dsr.2015.04.004>
- Jeffrey SW, Vesik M (1997) Introduction to marine phytoplankton and their pigment signatures. In: Jeffrey SW, Mantoura RFC, Wright SW (eds) *Phytoplankton pigments in oceanography*, 1st edn. UNESCO Publishing, Paris, pp 37–84
- Joo HM, Lee SH, Jung SW et al (2012) Latitudinal variation of phytoplankton communities in the western Arctic Ocean. *Deep-Sea Res II* 81:3–17. <https://doi.org/10.1016/j.dsr2.2011.06.004>
- Kawaguchi Y, Nishino S, Inoue J (2015) Fixed-point observation of mixed layer evolution in the seasonally ice-free Chukchi sea: turbulent mixing due to gale winds and internal gravity waves. *J Phys Oceanogr* 45:836–853. <https://doi.org/10.1175/JPO-D-14-0149.1>
- Kuwahara VS, Leong SCY (2015) Spectral fluorometric characterization of phytoplankton types in the tropical coastal waters of Singapore. *J Exp Mar Biol Ecol* 466:1–8. <https://doi.org/10.1016/j.jembe.2015.01.015>
- Lane PVZ, Llinás L, Smith SL, Pilz D (2008) Zooplankton distribution in the western Arctic during summer 2002: hydrographic habitats and implications for food chain dynamics. *J Mar Syst* 70:97–133
- Leu E, Søreide JE, Hessen DO et al (2011) Consequences of changing sea-ice cover for primary and secondary producers in the European Arctic shelf seas: timing, quantity, and quality. *Prog Oceanogr* 90:18–32. <https://doi.org/10.1016/j.pocean.2011.02.004>
- Li WKW, McLaughlin FA, Lovejoy C, Carmack EC (2009) Smallest algae thrive as the Arctic Ocean freshens. *Science* 326:539. <https://doi.org/10.1126/science.1179798>
- Lin I-I (2012) Typhoon-induced phytoplankton blooms and primary productivity increase in the western North Pacific subtropical ocean. *J Geophys Res* 117((1978–2012)):3039. <https://doi.org/10.1029/2011jc007626>
- Liu H, Dagg M (2003) Interactions between nutrients, phytoplankton growth, and micro- and mesozooplankton grazing in the plume of the Mississippi River. *Mar Ecol Prog Ser* 258:31–42
- Liu H, Dagg MJ, Strom S (2005) Grazing by the calanoid copepod *Neocalanus cristatus* on the microbial food web in the coastal Gulf of Alaska. *J Plankton Res* 27:647–662

- Lochte K, Ducklow HW, Fasham MJR, Stienens C (1993) Plankton succession and carbon cycling at 47°N 20°W during the JGOFS North Atlantic bloom experiment. *Deep-Sea Res II* 40:91–114. [https://doi.org/10.1016/0967-0645\(93\)90008-B](https://doi.org/10.1016/0967-0645(93)90008-B)
- MacIntyre HL, Lawrenz E, Richardson TL (2010) Taxonomic discrimination of phytoplankton by spectral fluorescence. In: *Chlorophyll a fluorescence in aquatic sciences: methods and applications*. Springer, Dordrecht, pp 129–169
- Mackey M, Mackey D, Higgins H (1996) CHEMTAX-A program for estimating class abundances from chemical markers: application to HPLC measurements of phytoplankton. *Mar Ecol Prog Ser* 144:265–283
- Markus T, Stroeve J, Miller J (2009) Recent changes in Arctic sea ice melt onset, freezeup, and melt season length. *J Geophys Res* 114:C12024
- Martini KI, Simmons HL, Stoudt CA, Hutchings JK (2014) Near-inertial internal waves and sea ice in the Beaufort Sea. *J Phys Oceanogr* 44:2212–2234. <https://doi.org/10.1175/JPO-D-13-0160.1>
- Matsuno K, Yamaguchi A, Hirawake T, Imai I (2011) Year-to-year changes of the mesozooplankton community in the Chukchi Sea during summers of 1991, 1992 and 2007, 2008. *Polar Biol* 34:1349–1360. <https://doi.org/10.1007/s00300-011-0988-z>
- Matsuno K, Ichinomiya M, Yamaguchi A et al (2014) Horizontal distribution of microprotist community structure in the western Arctic Ocean during late summer and early fall of 2010. *Polar Biol* 37:1185–1195. <https://doi.org/10.1007/s00300-014-1512-z>
- Matsuno K, Yamaguchi A, Nishino S et al (2015) Short-term changes in the mesozooplankton community and copepod gut pigment in the Chukchi Sea in autumn: reflections of a strong wind event. *Biogeosciences* 12:4005–4015. <https://doi.org/10.5194/bg-12-4005-2015>
- Nishino S (2013) R/V Mirai cruise report MR13-06. JAMSTEC, Yokosuka
- Nishino S, Kikuchi T, Yamamoto-Kawai M et al (2011) Enhancement/reduction of biological pump depends on ocean circulation in the sea-ice reduction regions of the Arctic Ocean. *J Oceanogr* 67:305–314. <https://doi.org/10.1007/s10872-011-0030-7>
- Nishino S, Kawaguchi Y, Inoue J et al (2015) Nutrient supply and biological response to wind-induced mixing, inertial motion, internal waves, and currents in the northern Chukchi Sea. *J Geophys Res* 120:1975–1992. <https://doi.org/10.1002/2014JC010407>
- Nishino S, Kikuchi T, Fujiwara A et al (2016) Water mass characteristics and their temporal changes in a biological hotspot in the southern Chukchi Sea. *Biogeosciences* 13:2563–2578. <https://doi.org/10.5194/bg-13-2563-2016>
- Rainville L, Woodgate RA (2009) Observations of internal wave generation in the seasonally ice-free Arctic. *Geophys Res Lett* 36:1487. <https://doi.org/10.1029/2009GL041291>
- Sato K, Aoyama M, Becker S (2010) Reference materials for nutrients in seawater as calibration standard solution to keep comparability for several cruises in the world ocean in 2000s. In: Aoyama M et al (eds) *Comparability of nutrients in the world's ocean*. Mother Tank, Tsukuba, pp 43–56
- Sepp M, Jaagus J (2011) Changes in the activity and tracks of Arctic cyclones. *Clim Chang* 105:577–595. <https://doi.org/10.1007/s10584-010-9893-7>
- Serreze MC, Walsh JE, Chapin FS et al (2000) Observational evidence of recent change in the northern high-latitude environment. *Clim Chang* 46:159–207. <https://doi.org/10.1023/A:1005504031923>
- Sherr EB, Sherr BF, Wheeler PA, Thompson K (2003) Temporal and spatial variation in stocks of autotrophic and heterotrophic microbes in the upper water column of the central Arctic Ocean. *Deep-Sea Res I* 50:557–571. [https://doi.org/10.1016/S0967-0637\(03\)00031-1](https://doi.org/10.1016/S0967-0637(03)00031-1)
- Sørdeide JE, Leu E, Berge J et al (2010) Timing of blooms, algal food quality and *Calanus glacialis* reproduction and growth in a changing Arctic. *Glob Chang Biol* 16:3154–3163. <https://doi.org/10.1111/j.1365-2486.2010.02175.x>
- Stroeve J, Holland MM, Meier W et al (2007) Arctic sea ice decline: faster than forecast. *Geophys Res Lett* 34:L09501. <https://doi.org/10.1029/2007GL029703>
- Sukhanova IN, Flint MV, Pautova LA et al (2009) Phytoplankton of the western Arctic in the spring and summer of 2002: structure and seasonal changes. *Deep-Sea Res II* 56:1223–1236. <https://doi.org/10.1016/j.dsr2.2008.12.030>
- Sunda W, Kieber DJ, Kiene RP, Huntsman S (2002) An antioxidant function for DMSP and DMS in marine algae. *Nature* 418:317–320. <https://doi.org/10.1038/nature00851>
- Suzuki R, Ishimaru T (1990) An improved method for the determination of phytoplankton chlorophyll using *N,N*-dimethylformamide. *J Oceanogr* 46:190–194. <https://doi.org/10.1007/BF02125580>
- Suzuki K, Minami C, Liu H, Saino T (2002) Temporal and spatial patterns of chemotaxonomic algal pigments in the subarctic Pacific and the Bering Sea during the early summer of 1999. *Deep-Sea Res II* 49:5685–5704
- Tremblay JÉ, Bélanger S, Barber DG et al (2011) Climate forcing multiplies biological productivity in the coastal Arctic Ocean. *Geophys Res Lett* 38:L18604. <https://doi.org/10.1029/2011GL048825>
- Uchimiya M, Motegi C, Nishino S et al (2016) Coupled response of bacterial production to a wind-induced fall phytoplankton bloom and sediment resuspension in the Chukchi Sea Shelf, Western Arctic Ocean. *Front Mar Sci* 3:533. <https://doi.org/10.3389/fmars.2016.00231>
- Van Heukelem L, Thomas CS (2001) Computer-assisted high-performance liquid chromatography method development with applications to the isolation and analysis of phytoplankton pigments. *J Chromatogr A* 910:31–49
- Vidussi F, Roy S, Lovejoy C et al (2004) Spatial and temporal variability of the phytoplankton community structure in the North Water Polynya, investigated using pigment biomarkers. *Can J Fish Aquat Sci* 61:2038–2052. <https://doi.org/10.1139/f04-152>
- Wang S, Ishizaka J, Hirawake T et al (2015) Remote estimation of phytoplankton size fractions using the spectral shape of light absorption. *Opt Express* 23:10301–10318. <https://doi.org/10.1364/OE.23.010301>
- Wang S, Xiao C, Ishizaka J et al (2016) Statistical approach for the retrieval of phytoplankton community structures from in situ fluorescence measurements. *Opt Express* 24:23635–23653. <https://doi.org/10.1364/OE.24.023635>
- Wright SW, Jeffrey SW (2006) Pigment markers for phytoplankton production. In: Volkman JK (ed) *The handbook of environmental chemistry*. Springer-Verlag, Berlin/Heidelberg, pp 71–104
- Yamamoto-Kawai M, Tanaka N, Pivovarov S (2005) Freshwater and brine behaviors in the Arctic Ocean deduced from historical data of $\delta^{18}O$ and alkalinity (1929–2002 A.D.). *J Geophys Res* 110:C10003. <https://doi.org/10.1029/2004JC002793>
- Yao W, Byrne RH (1998) Simplified seawater alkalinity analysis. *Deep-Sea Res I* 45:1383–1392. [https://doi.org/10.1016/S0967-0637\(98\)00018-1](https://doi.org/10.1016/S0967-0637(98)00018-1)
- Yentsch CS, Phinney DA (1985) Spectral fluorescence: an ataxonomic tool for studying the structure of phytoplankton populations. *J Plankton Res* 7:617–632. <https://doi.org/10.1093/plankt/7.5.617>
- Yentsch CS, Yentsch CM (1979) Fluorescence spectral signatures-characterization of phytoplankton populations by the use of excitation and emission spectra. *J Mar Res* 37:471–483
- Yokoi N, Matsuno K, Ichinomiya M et al (2016) Short-term changes in a microplankton community in the Chukchi Sea during autumn:

- consequences of a strong wind event. *Biogeosciences* 13:913–923. <https://doi.org/10.5194/bg-13-913-2016>
- Yoshida M, Horiuchi T, Nagasawa Y (2011) In situ multi-excitation chlorophyll fluorometer for phytoplankton measurements: technologies and applications beyond conventional fluorometers. OCEANS'11 MTS/IEEE KONA, Waikoloa, pp 1–4
- Zhang X, Walsh JE, Zhang J et al (2004) Climatology and interannual variability of arctic cyclone activity: 1948–2002. *J Clim* 17:2300–2317
- Zhao H, Shao J, Han G et al (2015) Influence of typhoon matsa on phytoplankton chlorophyll-*a* off East China. *PLoS ONE* 10:e0137863. <https://doi.org/10.1371/journal.pone.0137863>